

Optical, structural and morphological properties of CdS-CdCO₃ films.

M. Chávez Portillo^a, A. Sosa Sánchez^a, G. Juárez Díaz^{b,*}, L. A. Chaltel Lima^c, S. Cruz Cruz^d,
R. Gutierrez Pérez^c, G. Hernández Téllez^c and O. Portillo Moreno^{c,**}

^a*Centro de Investigaciones en Dispositivos Semiconductores,
Instituto de Ciencias, Benemérita Universidad Autónoma de Puebla.*

P. O. Box 1067, Puebla, Pue. 72001 México.

^b*Facultad de Ciencias de la Computación, Benemérita Universidad Autónoma de Puebla,*

P. O. Box 1067, Puebla, Pue. 72570 México,

**e-mail: j.gabriel@rocketmail.com*

^{c,**}*Lab. De Ciencias de Materiales, Facultad de Ciencias Químicas, Benemérita Universidad Autónoma de Puebla,*

P.O. Box 1067, Puebla, Pue. 72001 México,

***e-mail: osporti@yahoo.com.mx*

^d*Dpto. de Ing. Química, Universidad Politécnica de Tlaxcala,*

Av. Universidad Politécnica No.1, San Pedro Xalcaltzinco, Tepeyanco, Tlax. México.

Received 28 July 2014; accepted 12 January 2015

CdS-CdCO₃ thin films were grown by chemical bath deposition. Different constant deposition temperatures were employed in the range of 20-80°C. From X-ray Diffraction (XRD) results can be observed that intensity of CdS peak is abruptly reduced when deposition temperature is decreased. By SEM images the formation and change in shape and size of crystallites can be observed as temperature is decreased. The forbidden energy band gap was 2.4-4.1 eV, determined from optical absorption. The formation of products was further confirmed with FTIR studies.

Keywords: Deposition temperatures; Gibbs energy; coordination complex; Otavite; morphological.

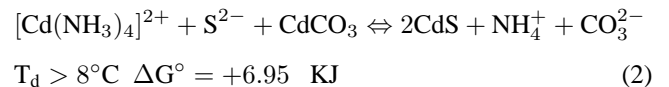
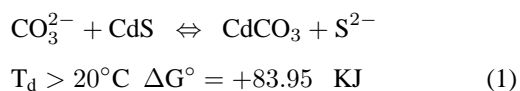
PACS: 06.60.-c; 61.05.cp; 78.40.-q.

1. Introduction

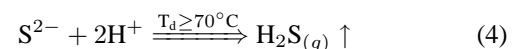
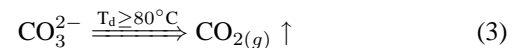
The size-and shape-dependent optical of semiconductors have motivated attempts to use as novel building blocks for optoelectronic methods are now accessible for preparing size- and shape-controlled crystals [1]. Structurally well-defined building blocks are potentially useful in the synthesis of designed catalysts, photonics band gap materials and chemical separations media [2]. The ability to understand and predict the final architecture building blocks is still limited. If we understand the growth mechanism and the shape-guiding process, will be possible to program the system to yield the building blocks with desired shape and crystallinity [3]. The cadmium carbonate (CdCO₃, Otavite), the physical properties of this material, alone or mixed with CdS, have scarcely been studied; can be useful in applications as insulators, composites, electrodes, sensors, among other devices. In this paper, we attempt elucidate the effect of deposition temperature (T_d) on morphological, structural and optical properties of CdS thin film growth by chemical bath (CB).

2. Chemical Reactions and experimental details

The growth of the CdS-CdCO₃ by CB is carried out according to the following stages [4,5,6].



However, in this case according to (2) and (1)



If $\Delta G^\circ > 0$, the reactions (1) and (2) are no-spontaneous. For chalcogenide semiconductors, the crystal size has been shown to be dependent on the deposition mechanism: the cluster mechanism result in smaller crystal size than the ion-ion mechanism. In the cluster mechanism, the size of the metal hydroxide colloids present in the deposition solution is expected to define the produced crystal size, and this size will depend largely on temperature [7]. For the ion-by-ion reaction, nucleation is generally slower and growth often occurs only at a solid surface and not (or at least much less) in the bulk of the solution [8]. The effect of temperature on crystal size is intuitively well-known, higher temperatures mean separate crystal faster diffusion on a substrate and interdiffusion between separate crystals, leading to larger crystals [2].

CdS-CdCO₃ crystalline thin films have been prepared on glass substrates at different deposition temperatures (T_d) 20-80°C range by CB. The following aqueous solutions were used for the growth of CdS-CdCO₃ layers: CdCl₂ (0.02 M),

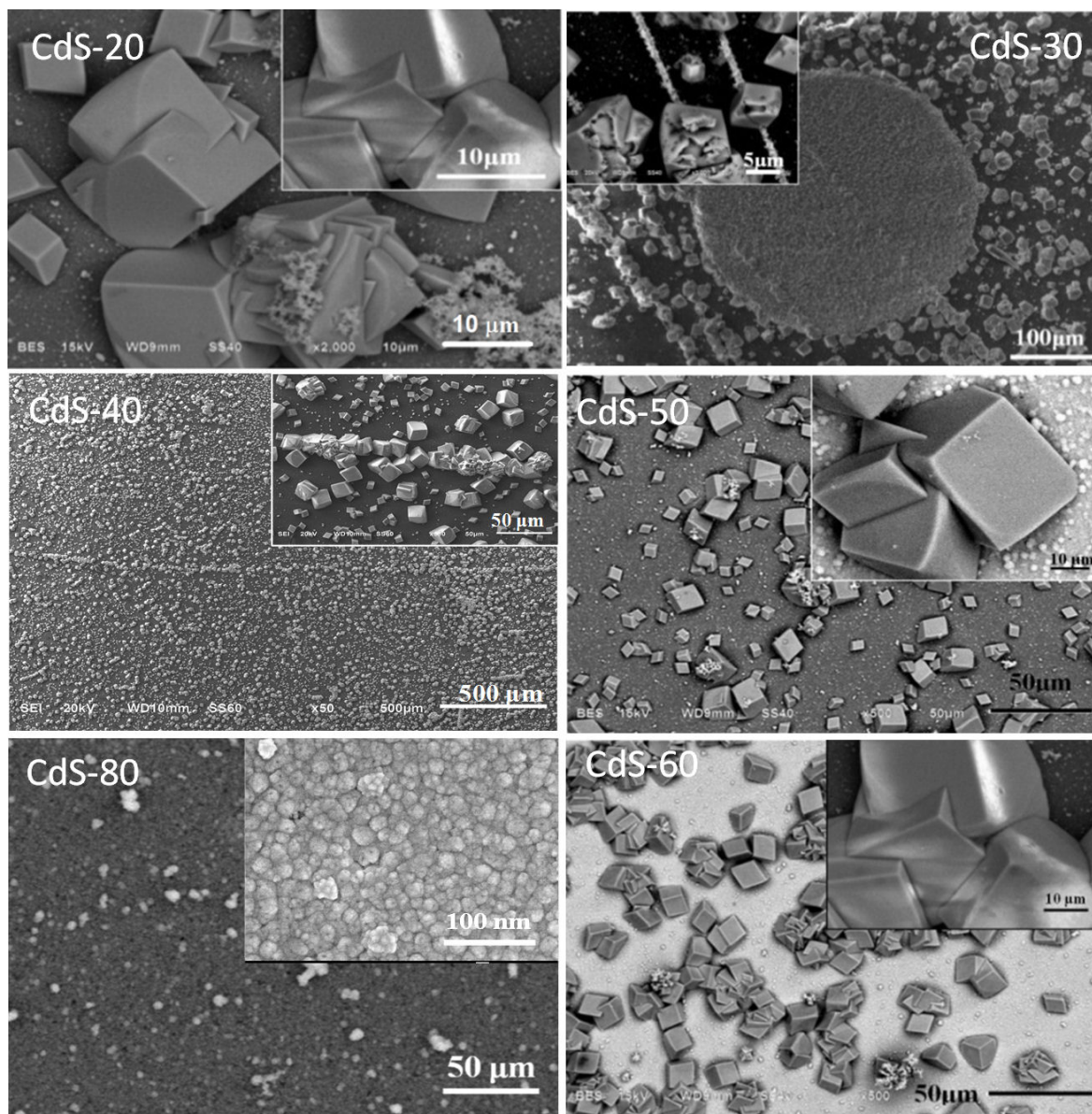


FIGURE 1. SEM micrographs with high-magnification and low-magnification images closely packed.

KOH (0.5 M), NH_4NO_3 (1.5 M), and $\text{SC}(\text{NH}_2)_2$ (0.02 M). The relative concentrations, volume proportions, stirring, T_d , and pH were kept constant during the growth process. The growing time was varied from 15 min to 24 h. The samples were labeled CdS80, CdS70, . . . , CdS20 to the deposited films with temperatures of 80 to 20°C in intervals of 10°C, respectively. Details of preparation were previously published [4,5,6,9].

Crystalline structure characterization was carried out by X-ray Diffraction (XRD) patterns registered in a Bruker D8 Discover diffractometer, using the $\text{Cu K}\alpha$ line. The optical absorption studies were carried out using UV-VIS-IR spectrophotometer (Cary-5000), to calculate the forbidden band gap energy (E_g) by using the $(\alpha h\nu)^2$ vs. $h\nu$ plot, where α is the optical absorption coefficient and $h\nu$ the photon energy.

The FTIR spectrum was recorded using a Perkin Elmer spectrophotometer in the wavenumber range of 500-4000 cm^{-1} .

3. Results and discussion

3.1. Scanning Electronic Microscopy (SEM)

The morphological analysis of the films was carried out in a scanning electronic microscope (SEM). Figure 1 shows micrographs with low-magnification and high-magnification SEM images closely packed. The image for CdS80 sample shows a typical image for CdS, polycrystalline film, observation of the film shows smooth surface and well adhesive nature of the film to substrate. However it can be seen in CdS60 that the products were cubes, when the T_d decreases, the mor-

phology and size of CdS show a variety of cubes-shaped, truncated cubes, wires and circles. The closely packed microcrystals with flat surfaces and sharp edges/corner are clearly showing in the magnification of SEM images. Inset of CdS50 sample show the SEM image, indicating that the slightly truncated cubes, this is square/cube facets. For CdS20 sample, these observations confirm that the circle consist of small crystals in perfectly aligned manners as found in many materials [10]. In order to explore the influence of different S^{2-} and CO_3^{2-} ions source and T_d on the morphology under some experimental conditions the following experiments were performed. (i) We employed thiourea as a S^{2-} and CO_3^{2-} ions source, CdS and CdCO₃ were obtained (ii) solid solution of CdS-CdCO₃ irregular particles were observed, when T_d parameter was decreased the cubes were formed. Irregular particles CdCO₃, the bigger cubes with $\sim 10 - 20 \mu\text{m}$ edge length were obtained. For CdS20 film an interesting feature shown is that each ring comprises numerous particles aggregating on the surface. At this point, the crystals in suspension are colloidal and adhered to form agglomerates into small clusters (or nuclei) due their thermodynamic stability. With a continuous supply of building cubes, secondary growth processes such as Ostwald ripening or aggregation resulting further growth to form larger circle, ring, and wire architectures. Thermodynamically, the combination of the building blocks mainly relies on two factors, namely, the surfaces energies and the lattice matching extent of the attached surfaces. It has been found that only the facets that have the same or similar surface energies and lattice orientations can attach together because at the interface, the crystals have the same lattice stripe orientation. CdCO₃ crystallites possess different shapes and orientation facets, the combination probability on the succeed crystallites will depend on the surface energies and structures of the crystallites. Generally, only the microcrystals with same or similar shapes attach together. With more and more cubes attaching to the existent CdCO₃ one by one in the same way, a chain-like structure is formed [6]. In general, decreased T_d is related to an enhance of size and quantity of CdCO₃ crystals, the large stacks are appreciated in CdS50 film. These images show that for CdS60 there are still round particles with lateral size $\sim 20 \mu\text{m}$, but in addition, some faceted, rectangular particles appear. This abrupt transition in a crystal size and morphology occurring with a decreasing of T_d suggests a change in the deposition mechanics, further increase in T_d result in complete transition to be faceted regular. In the assembly of nanoparticles, with the surfactants on the surface can be traded as hard cubes, and the arrangement of the particles obeys the traditional prediction in a crystal model, were the structures of the crystals are quite predictable on the basis of the ratio of the sizes of different units in the assembly of nanoalloys of different nanoparticles [11]. The assembly of anisotropic nanostructures, including nanotubes and nanowires, requires more effort and remains as a good challenge. Fortunately, recent progress demonstrated the good manipulation on the assembly of these more complex struc-

tures, including nanorods and nanowires. Ordered chains of BaCrO₄ were observed and assembly of these structures was attributed to interactions between the surfactants on surface of the adjacent nanorods [12]. Nikoobakht and co-worker suggested that in the assembly of nanorods, the interacting forces determining the parallel alignment between nanorods include higher lateral capillary forces along the length of the nanorods than its width, and van der Waals attraction and a screened Coulomb repulsion between nanorods [13]. Besides the directional capillarity force and van der Waals attraction, the consideration that the maximization of the entropy of the self-assembled structures by minimizing the excluded volume per particle in array by Onsager was also taken into account in their explanation. We report here of self-assembled cubes, the Waals of which enclose CdS particles as building units. Such cubes involved metastable structures in system CdCO₃. It has also been suggested that rotation and subsequent collisions of particles, driven by random thermal motions, my align the particles and lead to removal of adjacent crystal surfaces. The dipole-dipole interaction of the neighboring particle may also play an important role in aligning the crystals [14]. Unquenched dipole moments of neighboring particles drive the rotation of particles. It should also be noted that since the layers govern the crystal morphologies, the crystal cannot be expected to be random powders even at low T_d ; they should have some grade of preferential alignment. Thus, the rotation angles required to perfectly align the crystal are small. Further, even a slight preferential orientation, at low T_d , will bias the orientation during the alignment at the interface in a particular direction. Enhanced alignment via oriented attachment of preformed particles is only possible explanation for our observations. However, it is difficult to understand the bending behavior that leads to cubes using second mechanism proving or disproving mechanisms in this

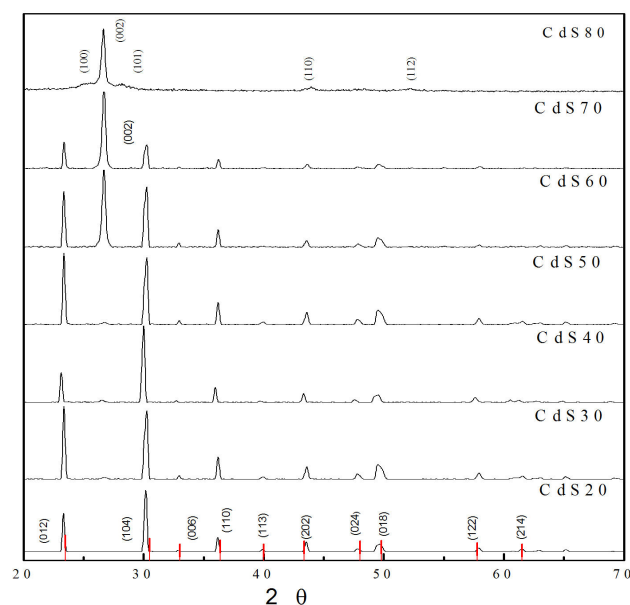


FIGURE 2. X-ray diffraction patterns of CdS20-80 films.

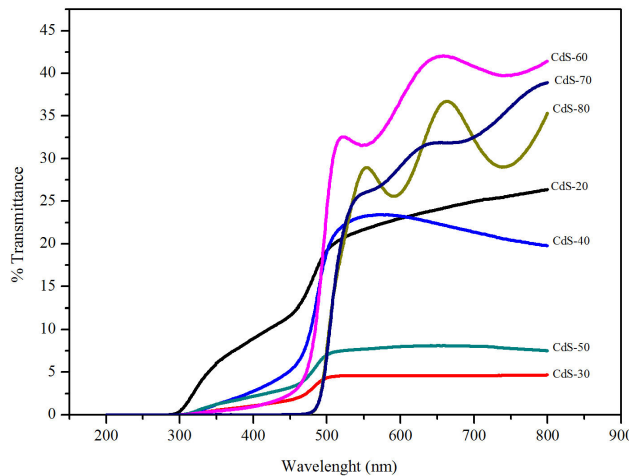


FIGURE 3. Transmission spectra of CdS20-80 layers.

this complex system and following the cube formation process step-by-step is unfortunately quite difficult since several different kinds of particles coexisting in every point in films.

3.2. X-ray diffraction (XRD)

XRD CdS80-20 patterns are illustrated in Fig. 2. The CdS-80 film presents the hexagonal wurtzite (WZ) crystalline phase [14]. The two small peaks at both sides of (002) central reflection define the triplet that distinguishes at hexagonal phase from cubic zincblende (ZB) structure in CdS [JCPDS-ICDD X-ray cards 10-454 and 06-314]. CdS20 sample show the XRD peaks located in: $2\theta = (23.4, 30.2, 36.4, 40.1, 43.8, 48.0, 49.5, 49.9, 58.2, 61.7, 62.9, 65.5)$, were indexed by assigning them otavite which has rhombohedral crystalline structure [JCPDS 042-1342]. In addition, the XRD revealed than the cube like structured CdCO_3 crystals tended to grow preferentially along (104) direction [14].

3.3. Optical absorption

The transmission spectra in the wave range 200-800 nm of Cd20-80 layers are shown in Fig. 3. This show a shift of their transmission edges to low wavelength. Films CdS60 had better optical quality, which is evident from sharp fall in transmission at the absorption edge, indicating better crystallinity of the films. The absorbance is very small and the transmission 80%, which indicates that the sample has a minimum lattice defects. However, the parallel transmission shift indicates that are related to changes in films structure. The increase in transmittance with increase in UV-region is not sharp. This fact indicates that the absorption band gap transition in the films are due to direct transitions [15]

$$(E - E_g)^{\frac{1}{2}} = \alpha h\nu \quad (5)$$

and an extrapolation to $\alpha^2 = 0$ yields is a good approximation of the forbidden band gap (E_g). Optical absorption

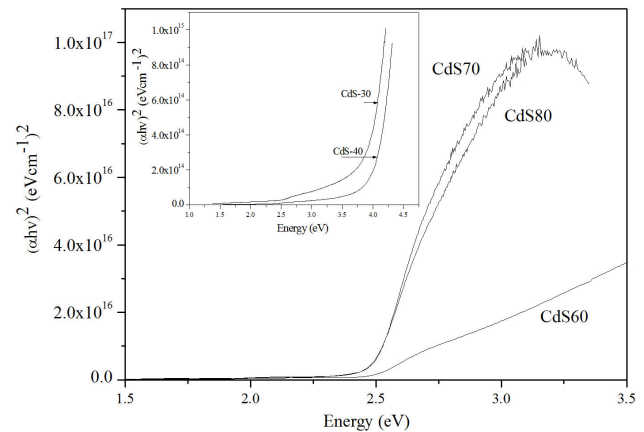


FIGURE 4. $(\alpha h\nu)$ versus $h\nu$ plot for CdS80-60, films. Inset shows CdS-40, CdS-30 films absorption.

spectra allow to calculate E_g for all the films. Optical absorption spectra allow to calculate E_g for all the films. Figure 4 exhibits $(\alpha h\nu)^2$ versus $h\nu$ plot for CdS80-20 films. The inset in the upper right part of the same plot shows the spectrum of absorption for the samples CdS-30 and CdS40 respectively. For CdS60 sample, two linear parts can be extrapolated in two values of direct E_g are defined. All this behaviour is an indication that for CdS60, both materials are aggregated one from another one [5]. These spectra exhibit different features depending on the morphological variation, the absorption spectra of CdS80-20 properties of crystals are generally impacted by many factors, such particle shape, size, and size distribution. In particular, the effect of lattice defect could be ignored. It is thought that the samples with longer crystalline have low concentration of defects, which act at sites for non radiative recombination of electron-hole pair. Another particularity observed in Fig. 4 is the presence of band-tail absorption. This phenomenon is due to existence of a tail density if gap state in degenerate materials, which has been attributed to local mechanical stress produced by impurities exhibits and exponential dependence on photon energy $\alpha(\omega)\alpha \exp(\hbar\omega - \hbar\omega_0)/E_0$, being a characteristic increases with de impurity concentration [15], were $\hbar\omega$ is the photon energy and E_0 and $\hbar\omega_0$ are fitting parameters, E_0 being proportional to kT .

3.4. Fourier transforms infrared spectra (FTIR)

Fourier transforms infrared spectra (FTIR) technique, can be employed to establish the identity of the compounds or determine the structure of new compounds. In revealing the structure of new compounds, FTIR is quite useful to predict the presence of certain functional group which absorbs defined frequencies. Figure 5 shows FTIR spectra CdS80-20 layers. The main spectral features are similar except for the intensity of the 1717-1384 cm^{-1} absorption bands. The peaks around 1400 cm^{-1} , 850 cm^{-1} and 718 cm^{-1} are characteristics vibration bands of CO_3^{2-} [1]. The absorption bands attributed to the vibrations in CO_3^{2-} anion are located within the 3600-400 cm^{-1} region. The strong broad absorption centered at

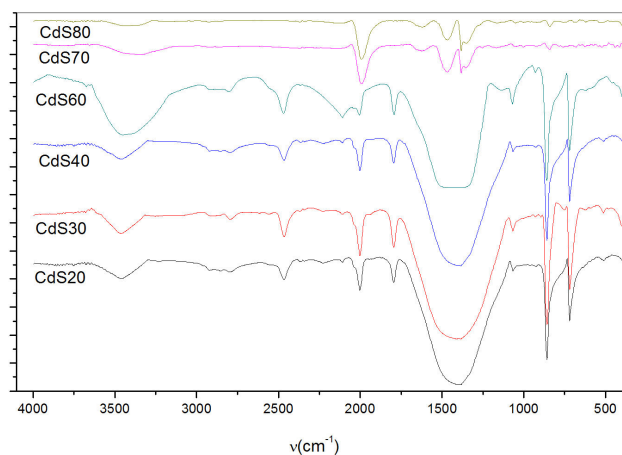


FIGURE 5. Fourier transforms infrared spectra (FTIR) for CdS80-20 samples.

at about 1448 cm^{-1} is connected with the asymmetric stretching vibrations and strong sharp absorption band at 852 cm^{-1} is assigned to the bending out plane vibrations. The broad absorption band in the $3385\text{-}3304\text{ cm}^{-1}$ region can be attributed to stretching of the -OH groups of defective sites and the physically adsorbed water molecules. We found FTIR absorption bands at about 3400 cm^{-1} caused by hydroxyl groups [16,17]. Two FTIR bands were observed at 1466 and 1548 cm^{-1} , which are attributed to symmetric and

asymmetric stretching vibrations of the carboxylate groups respectively. All the samples showed a sharp stretching mode at can be seen at 1384 cm^{-1} , vibration mode of $\text{NH}_4^+ \text{CO}_3^{2-}$, see Eq. (1) and (2). A large band around 1500 cm^{-1} corresponds to the stretching frequency of $\text{NH}_4^+ \text{CO}_3^{2-}$ surface groups, which were observed in FTIR spectra [18].

4. Conclusions

By SEM micrographs is observed that cubes with different shapes are formed on surface of CdS. The cubes are constituted by CdCO₃, also was observed the assembly of cubes forming diverse structures like chains, rings and circles. The dipole-dipole interaction of the cubes is the most likely mechanism that produce the arrangements. XRD peaks at $2\theta = (23.4, 30.2, 36.4, 40.1, 43.8, 48.0, 49.5, 49.9, 58.2, 61.7, 62.9, 65.5)$ reveals that films has rhombohedral crystalline structure corresponding to CdCO₃ (otavite) compound, temperature changes the XRD peaks producing a transformation to CdS. The optical absorption measurements determines that E_g increase 2.4-4.1 eV as the CdCO₃ is formed. The main spectral FTIR features are similar for samples except the intensity of the $1717\text{-}1384\text{ cm}^{-1}$ absorption band and the peaks around 1400 cm^{-1} , 850 cm^{-1} and 718 cm^{-1} which are characteristics vibration bands of CO_3^{2-} which corresponding to transformation of $\text{CdS} \rightarrow \text{CdCO}_3$.

1. C. Gao, W. Zhang, H. Li, L. Lang, and Z. Xu, *Cryst. Growth Des.* **8** (2008) 3785.
2. G. Hodes, *Phys. Chem. Chem. Phys.* **9** (2007) 2181.
3. G.A. Ozin, *Adv. Mater.* **4** (1992) 612.
4. O. Portillo Moreno, H. Lima Lima, R. Lozada Morales, R. Palomino Merino, O. Zelaya Ángel, *J. of Mat. Sci.* **40** (2005) 4489.
5. O. Portillo Moreno *et al.*, *J. of Mat. Sci. and Engin.*, **A1** (2010) 692.
6. R. Melendrez Luevano, *et al.*, *J. of Mat. Sci. and Engin.*, **A3** (2013) 289.
7. M. Kokotov and G. Hodes, *Chem. Mater.* **22** (2010) 5483.
8. S. Gorer and G. Hodes, *J. Phys. Chem.* **98** (1994) 5338.
9. M. Chavez Portillo, L.A. Chaltel Lima, U. Peña Rosas, G. Hernandez Tellez, R. Gutierrez Pérez, O. Portillo Moreno, *Materials Letters* **120** (2014) 130-132.
10. S. Ashoka, G. Nagaraju, K.V. Thipperudraiah, G.T. Chandrappa, *Materials Research Bulletin* **45** (2010) 1736.
11. C. Kiely, J. Fink, J.G. Zheng, M. Brust, D. Bathell, D.J. Schiffrin, *Adv. Mat.* **12** (2000) 640.
12. P. Yang and F. Kim, *Chem. Phys. Chem.* **3** (2002) 503.
13. B. Nikoobakht, Z.L. Wang, M.A. El Sayed, *J. Chem. Mater.* **B 15** (2003) 1957.
14. M. Becerril, *et al.*, *Mat. Res.*, **15** (2012) 1.
15. O. Portillo Moreno *et al.*, *J. of Electrochem. Soc.* **153** (2006) 926.
16. S. John, C. Soukoulis, M.H. Cohen and E.N. Economou, *Phys. Rev. Lett.* **57** (1986) 1777.
17. S. Ashoka, G. Nagaraju, K.V. Thipperudraiah, G.T. Chandrappa, *Mat. Res. Bull.* **45** (2010) 1736.
18. R. Palomino Merino, O. Portillo Moreno, L.A. Chaltel Lima, R. Gutierrez Pérez, M. De Icaza Herrera and V. Castaño, *J. of Nanomaterials*, **2013** (2013) ID 507647.